Bulletin of the Seismological Society of America, Vol. 101, No. 5, pp. 2355–2368, October 2011, doi: 10.1785/0120100295

Ⓔ

Similarities and Differences in the Rupture Process of the $M \sim 4.8$ Repeating-Earthquake Sequence off Kamaishi, Northeast Japan: Comparison between the 2001 and 2008 Events

by Kouhei Shimamura, Toru Matsuzawa, Tomomi Okada, Naoki Uchida, Toshio Kono, and Akira Hasegawa

Abstract Earthquakes of $M \sim 5$ have repeatedly occurred at the same location on the plate boundary off Kamaishi, northeast Japan, with a mean recurrence interval of about 5.5 years. The latest two events (M 4.8 on 13 November 2001, and M 4.7 on 11 January 2008) were successfully observed by the broadband seismic network of Tohoku University covering the Tohoku District of northeast Japan. We estimated the source processes of the 2001 and 2008 events by carefully picking the onsets of P and S waves and by inverting seismic waveforms recorded by the network. The results show that both events were caused by the rupture of the same asperity patch (diameter, ~1 km). As the previous 1995 event was also reported to have ruptured the source area of the 2001 event, at least the last three events (1995, 2001, and 2008) in this earthquake sequence are thought to have been caused by repeated ruptures of the same asperity. A closer examination, however, reveals a small discrepancy in the slip distribution between the last two events, which explains the difference in the high-frequency components of the seismograms. The regions in which slip was smaller during the 2001 event than during the 2008 event nearly coincide with the source areas of the smaller repeating earthquakes that occurred just before the 2001 event. This finding suggests that the activity of smaller events immediately before the mainshock can influence the slip distribution of the mainshock.

Online Material: Figures of waveform fit, slip model using an alternative EGF, and test of stability of slip amount.

Introduction

Recently, the asperity model has been reevaluated to ensure it is appropriate for describing how earthquakes occur on plate boundaries at subduction zones. The asperity model was first proposed by Kanamori and coworkers (Lay and Kanamori, 1980; Kanamori, 1981; Lay and Kanamori, 1981; Lay *et al.*, 1982) in terms of heterogeneities of stress (strength) distributions to explain the varied occurrence patterns of large earthquakes in circum-Pacific subduction zones. In the model, asperities correspond to areas with high strength relative to the surroundings. On the asperities, stresses are repeatedly concentrated due to tectonic loading and are released by earthquakes. Therefore, the asperity model predicts that very similar earthquakes may occur repeatedly on an asperity if it is isolated from other asperities.

Geller and Mueller (1980) reported that four small earthquakes on the San Andreas fault had similar waveforms and suggested that they might be caused by ruptures of the same asperity, where stress was repeatedly concentrated and then released. Moreover, microearthquakes occur regularly in many clusters on the San Andreas fault at Parkfield, California (Ellsworth, 1995; Nadeau *et al.*, 1995; Nadeau and McEvilly, 1997) and in the northeastern Japan subduction zone (Igarashi *et al.*, 2003). The microearthquakes in each cluster show nearly identical waveforms, and their hypocenters are closely located. Thus, these earthquakes are regarded as the repeated ruptures of the respective asperities and are called repeating earthquakes.

Following its initial development, the asperity model has been interpreted and modified in terms of rate- and state-dependent friction laws (e.g., Scholz, 1990; Boatwright and Cocco, 1996). In the modified asperity model, a plate boundary is divided into two types of regions: stably sliding regions and asperities. The stably sliding regions correspond to rate-hardening areas that usually slip aseismically, whereas asperities are rate-weakening regions that always slip seismically. The stress at an asperity builds up as the surrounding regions

slip aseismically, and eventually the asperity ruptures, causing an earthquake. During the rupture process, the stably sliding regions act as barriers that restrain rupture propagation because of their rate-hardening nature. Therefore, most of the coseismic slip is concentrated on asperities, meaning that they can be imaged from the slip distributions estimated from seismic waveform inversions (e.g., Yamanaka and Kikuchi, 2003; Yagi, 2004; Wu *et al.*, 2008).

Nagai *et al.* (2001) estimated the slip distributions of the 1968 Tokachi-oki earthquake (M 7.9) and the 1994 Sanriku-haruka-oki earthquake (M 7.6) by applying the same inversion method to the waveform data from almost the same station sets for both events. They found that the 1968 Tokachi-oki earthquake was caused by the rupture of two (northern and southern) asperities and that the southern asperity was ruptured again in the 1994 Sanriku-haruka-oki earthquake. Yamanaka and Kikuchi (2004) showed that the southern asperity was also ruptured during a 1931 event (M 7.2). Yamanaka and Kikuchi (2003) also estimated the rupture areas of the 1952 (M 8.2) and 2003 (M 8.0) Tokachi-oki earthquakes, revealing that most of the rupture areas of the two events overlapped with each other, indicating that the 2003 event was caused by the rupture of the same asperity as for the 1952 event. Yaginuma *et al.* (2007) estimated the coseismic slip distribution of the 2005 Miyagi-oki earthquake (M 7.2). By comparing their result with the previously derived results for the 1978 Miyagi-oki earthquake (M 7.4) (e.g., Yamanaka and Kikuchi, 2004), they showed that the rupture extent of the 2005 event overlapped with the southeastern part of the source area for the 1978 event. This result suggests that three asperities cause the sequence of Miyagi-oki earthquakes; the 2005 event ruptured one of these asperities, while the 1978 event ruptured all three asperities simultaneously.

The results of many studies, including those mentioned previously, suggest that the asperity model can be used to explain the occurrence of earthquakes at a plate boundary in subduction zones (e.g., Okada *et al.*, 2003). However, the model may be too simple to explain the variety of seismic slip observed at plate boundaries. For example, Park and Mori (2007) and Konca *et al.* (2008) argued that seismic patches showing large seismic slip are not always the same patch within the locked area in the interseismic period. Therefore, the asperity model needs to be refined to explain the variation in slip distribution for events occurring at a given location.

A sequence of repeating earthquakes of $M \sim 5$ off Kamaishi, Iwate prefecture, Japan (Matsuzawa *et al.*, 1999, 2002), provides a good opportunity to investigate the reproducibility of the slip distribution in the repeated rupture of the same asperity. Figure 1 shows a magnitude-time (M-T) diagram of earthquakes in the cluster that includes the $M \sim 5$ repeating earthquakes off Kamaishi. By comparing the rupture area of the 2001 event with that of the 1995 event estimated by waveform inversions, Okada *et al.* (2003) showed that most of the rupture areas of the two events overlap with each other. The authors concluded that the two events were caused by repeated ruptures of the same asperity.

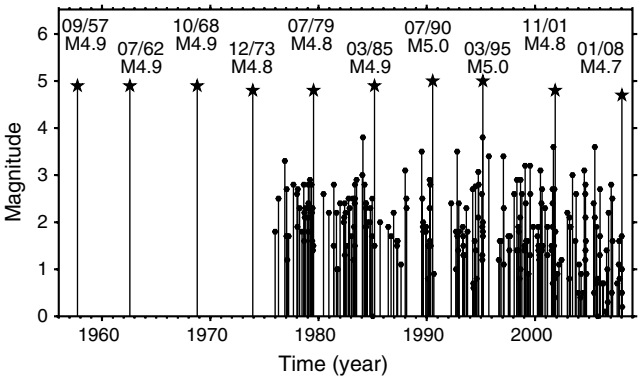

Figure 1. Magnitude-time (M-T) diagram of the repeating earthquakes off Kamaishi (stars) and background microearthquakes (hexagons) (Uchida *et al.*, 2007, 2008). The numbers above each star indicates the month and year when the event occurred (mm/yy) and the magnitude of the event.

Uchida *et al.* (2007) showed that smaller repeating earthquakes (asperities) exist in and around the larger asperity that generates the repeating $M \sim 5$ earthquakes off Kamaishi, suggesting a hierarchy of asperities. Hori and Miyazaki (2010) successfully reproduced the earthquake cycle at the asperities, with such a hierarchical structure, in a numerical simulation.

On 11 January 2008, an earthquake of M 4.7 occurred in the cluster within the time and magnitude ranges predicted by Matsuzawa *et al.* (2002). Figure 2 shows examples of seismograms of the 2001 and 2008 events with waveforms of vertical components (UD) in the frequency range of 1.0–5.0 Hz. The waveforms of the 2001 and 2008 events are very similar to each other in this frequency range. Okada *et al.* (2003) investigated the 1995 and 2001 events using the seismograms in this frequency range because of the low sampling rate for the 1995 event. The waveform data of the 2001 and 2008 events are much better than the 1995 event in both quality and quantity. These superior data enable us to investigate not only similarities but differences between the last two events in the sequence, which is not possible in comparing the 1995 and 2001 events.

In this paper, we estimated the moment release distributions of the 2001 and 2008 events by a waveform inversion method to compare the rupture processes of the two events in detail. Moreover, we compared our results with the locations and activities of smaller repeating earthquakes that occur around the two events, as estimated by Uchida *et al.* (2007, 2008).

Data and Method

We used three-component velocity-type seismograms obtained from Tohoku University's broadband-seismograph and microearthquake-observation networks. A three-component STS-1/VBB, STS-2 or short-period (1 s) seismometer was deployed at each station. The sampling

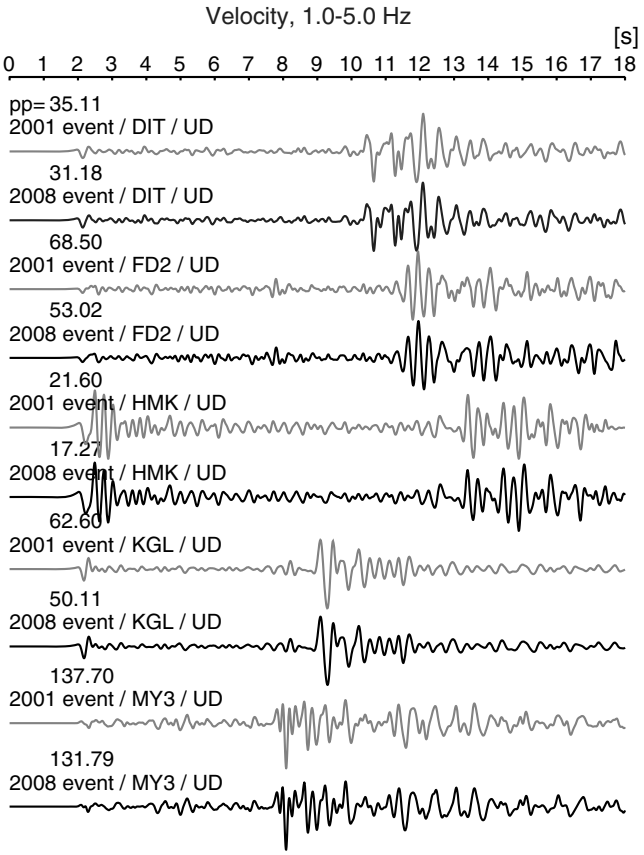

Figure 2. Examples of vertical-component (UD) waveforms of the 2001 (gray) and 2008 (black) events. All the waveforms are filtered with a pass-band of 1.0–5.0 Hz. The number above each waveform denotes the peak-to-peak amplitude (10^{-3} cm/s). The three-letter station code is shown above each waveform (see Fig. 3 for station locations).

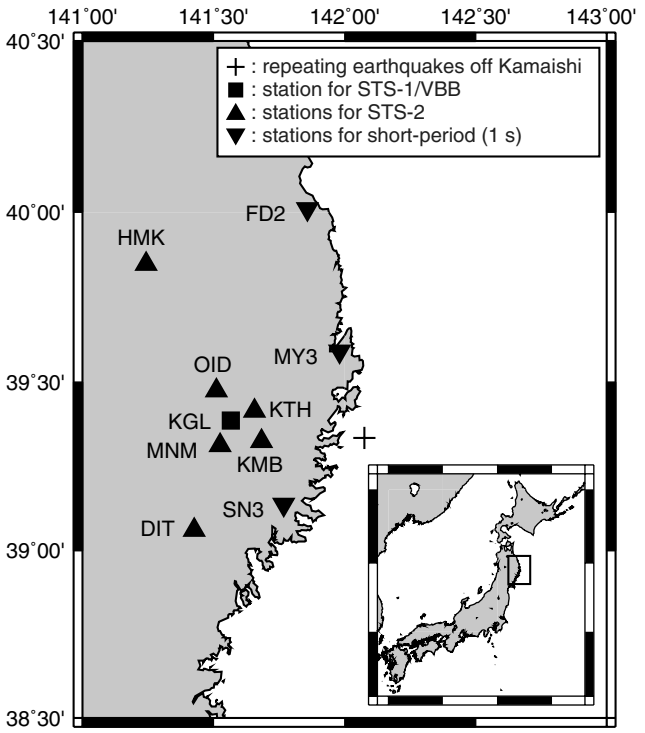

Figure 3. Locations of the stations used in this paper. Solid symbols indicate the types of seismometers deployed: squares for STS-1/VBB, triangles for STS-2, and inverted triangles for short-period (1-second) seismometers. Cross shows the location of the repeating-earthquake cluster off Kamaishi. The bottom right inset shows a map of the Japanese islands. The rectangle in the inset denotes the study area.

frequency is 100 Hz for all seismograms. Figure 3 shows the locations of the stations used in our analysis. The hypocentral parameters of the 2001 and 2008 events are listed in Table 1.

For estimating moment release distributions on the fault planes of the 2001 and 2008 earthquakes off Kamaishi, we used the multiple time-window waveform inversion method (Hartzell and Heaton, 1983). In this method, many grid points are distributed on an assumed fault plane and the observed waveforms are inverted to determine the moment release histories at respective grid points. In the inversion, the rupture front is assumed to propagate circularly at the maximum rupture velocity, and the moment rate function for each grid point is assumed to be expressed as a linear combination of some isosceles triangles with a base length of τ. The interval between isosceles triangles is set to half of τ. Thus, the unknown parameters are the heights of these isosceles triangles.

To stabilize the inversions, we applied *a priori* constraints on the smoothness of temporal and spatial changes and on the absolute values of unknown parameters. For the smoothness of temporal changes, second-order time-derivatives of unknown parameters were assumed to be small at each grid point. For the smoothness of spatial changes, two-dimensional Laplacians of unknown parameters were also assumed to be small. A weak damping was adopted because

Table 1
Focal Parameters for Repeating Earthquakes off Kamaishi and Events Used as Empirical Green's Functions (EGFs)*

Earthquake (mm/dd/yyyy)	Latitude (°)	Longitude (°)	Depth (km)	Magnitude
Off Kamaishi event (11/13/2001)	39.337	142.068	48.0	4.8
Off Kamaishi event (01/11/2008)	39.340	142.067	47.1	4.7
EGF (08/17/2001)	39.337	142.075	47.7	2.7
Alternative EGF (10/14/2001)	39.340	142.065	46.9	2.7

*All parameters are from the unified catalog of the Japan Meteorological Agency (JMA).

we found that such a damping was effective in constraining the unknown parameters to positive values, even if we did not apply the explicit positive constraints. Thus, we adopted the smallest smoothing and damping factors that constrain the parameters to nonnegative values.

For calculating Green's function, an empirical Green's function (EGF) method (e.g., Hartzell, 1978) was adopted. The event used as an EGF is the same as that employed by Okada *et al.* (2003): an M 2.7 event that occurred on 17 August 2001. Information on this event is shown in Table 1.

Parameters used in the inversions are described in detail in Waveform Inversion Analysis.

Picking First Arrivals

The rupture durations of the 2001 and 2008 repeating earthquakes off Kamaishi were estimated to be about 0.3 s, based on the inversions (see the discussion that follows). This means that we have to pick first arrivals with errors less than ~0.03 s to estimate the rupture processes in detail. However, it is very difficult to pick the first arrivals of S waves with such accuracy without *a priori* information. To achieve such accuracy, we picked onsets very carefully, taking into consideration that a double difference (DD) of S-wave arrival times should be the product of the DD of P-wave arrival times and the V_P/V_S ratio:

$$(t^1_{S,a} - t^1_{S,b}) - (t^2_{S,a} - t^2_{S,b}) = \gamma[(t^1_{P,a} - t^1_{P,b}) - (t^2_{P,a} - t^2_{P,b})], \quad (1)$$

where t_P and t_S are the arrival times of P and S waves, respectively; γ is the V_P/V_S ratio; superscripts (1 and 2) denote earthquakes; and subscripts (a and b) indicate stations. Equation (1) is derived as follows. In the case of earthquake 1 and two stations (a and b), the S-wave travel time is related to the P-wave travel time using γ:

$$t^1_{S,a} - t^1_O = \gamma(t^1_{P,a} - t^1_O), \quad (2)$$

$$t^1_{S,b} - t^1_O = \gamma(t^1_{P,b} - t^1_O), \quad (3)$$

where t^1_O is the origin time of earthquake 1. Subtracting equation (3) from equation (2), we obtain

$$t^1_{S,a} - t^1_{S,b} = \gamma(t^1_{P,a} - t^1_{P,b}). \quad (4)$$

Here, we can eliminate the origin time, which has an error as large as 0.1 s. Similarly, for earthquake 2, we obtain

$$t^2_{S,a} - t^2_{S,b} = \gamma(t^2_{P,a} - t^2_{P,b}). \quad (5)$$

Subtracting equation (5) from equation (4), we obtain equation (1). Moreover, we can transform equation (1) as follows:

$$(t^1_{S,a} - t^2_{S,a}) - (t^1_{S,b} - t^2_{S,b}) = \gamma[(t^1_{P,a} - t^2_{P,a}) - (t^1_{P,b} - t^2_{P,b})]. \quad (6)$$

Note that the DD is, at the maximum, as large as twice the time needed for the seismic wave to travel from hypocenter 1 to hypocenter 2.

In this paper, earthquakes 1 and 2 in equation (1) correspond to the repeating earthquake off Kamaishi with $M \sim 5$ and a small event used as an EGF, respectively. The hypocenters of these two events were estimated to be located within 1 km of each other (Uchida *et al.*, 2007, 2008), and V_P was estimated to be ~7.8 km/s at a depth of 50 km (Hasegawa *et al.*, 1978). Thus, the DD of P waves is estimated to be less than 0.3 s. As a result, the uncertainty in the DD of S waves in equation (6) is less than about 0.03 s, even if the spatial variation in the V_P/V_S ratio is as large as 10%.

However, there are eight unknown parameters in equation (1). Therefore, to pick a first arrival using equation (1), we must correctly pick seven other first arrivals, including S waves. Therefore, we adopted only the concept of equation (1): that a DD of S-wave arrival times should be the product of the DD of P-wave arrival times and the V_P/V_S ratio. The complete process is as follows.

1. Pick P- and S-wave arrival times for all stations.
2. Select a reference station.
3. Calculate the DDs of P- and S-wave arrival times for pairs consisting of the reference station and other stations.
4. Plot the DDs in a diagram with P-wave DDs on the horizontal axis and S-wave DDs on the vertical axis.
5. If all of the data are correctly picked, the points should be distributed along a line with a slope corresponding to the V_P/V_S ratio (γ).
6. If some points are plotted away from the line, repick the data.

Moreover, we took particle motions into consideration when picking arrival times.

We selected station KGL as the reference. Figure 4a shows the relation between the DDs of P waves and S waves for the pair consisting of the 2001 event and the EGF event. Figure 4b shows the same plot for the pair consisting of the 2008 event and the EGF event. Most of the data are located within about 0.03 s of the best-fit lines. Thus, we used these P- and S-wave arrival times in the waveform inversions.

Waveform Inversion Analysis

Analysis in the Frequency Range of 1.0–5.0 Hz

As shown in Figure 2, waveforms for the 2001 and 2008 events are very similar in the frequency range of 1.0–5.0 Hz. To confirm whether the 2008 event was caused by the same asperity as the 2001 event, we analyzed the data in this frequency range by using the same method as Okada *et al.* (2003), who analyzed the 1995 and 2001 events.

Parameters used for the inversions are as follows. Waveform data were resampled at a rate of 50 Hz and were band-pass filtered with a frequency range of 1.0–5.0 Hz. We used seismograms of 5-s time-windows starting from 2 s

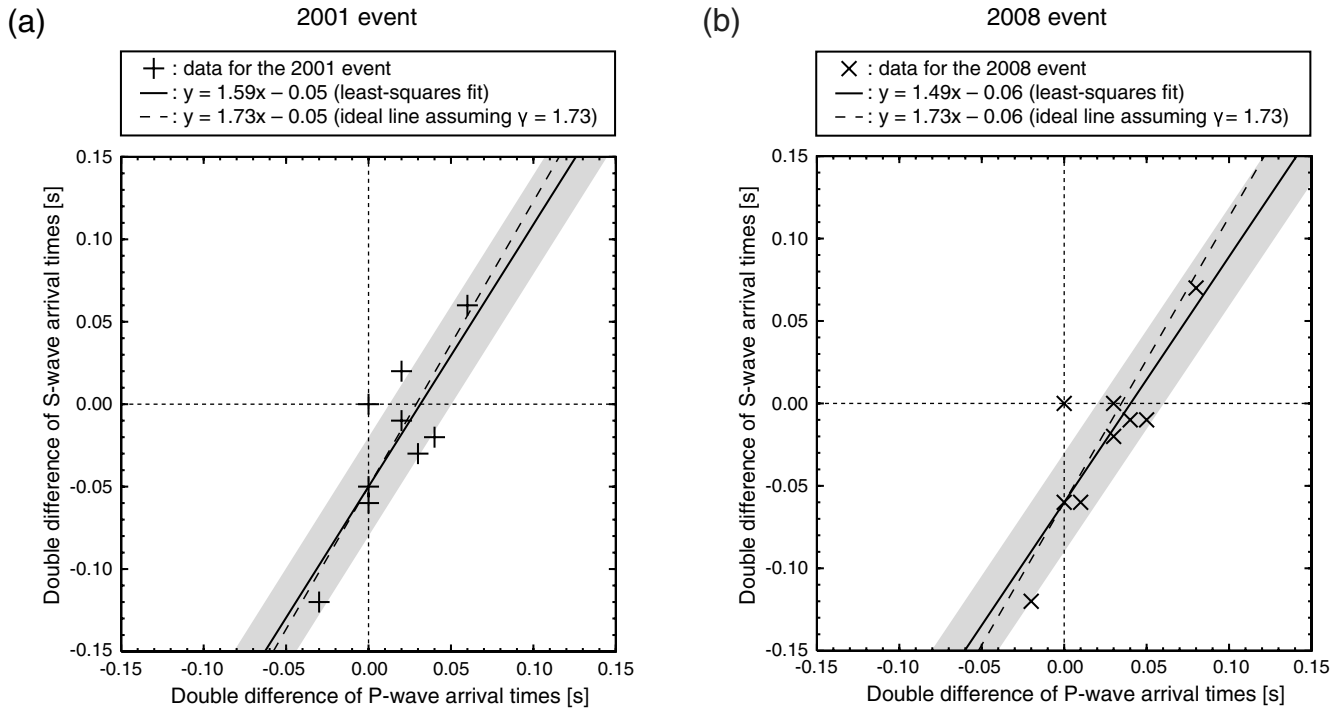

Figure 4. Relation between the double differences (DDs) of *P*-wave and *S*-wave arrival times. (a) Relation for the pair comprising the 2001 event and the EGF event. Crosses denote the DD data. Solid line indicates the least-squares fit line, and dashed line shows an ideal line for $\gamma(V_P/V_S) = 1.73$. The gray area indicates the range within ±0.03 s in the y-direction (DDs of *S*-wave data) from the least-squares fit. Here, we show the range based on the error in the y-direction because it is more difficult to pick *S*-wave arrival times than *P*-wave arrival times. (b) Relation between the DDs for the pair comprising the 2008 event and the EGF event. Crosses, solid line, dashed line, and gray area are the same as in (a).

before *P*- and *S*-wave arrivals. For the fault plane, we assumed that the maximum size was 2.4×2.4 km^2, and the geometry (strike, dip, rake) was (216°, 31°, 90°) according to the moment tensor inversion results presented by Okada *et al.* (2003). Grid points were placed on the fault plane with a spacing of 0.3 km in both the strike and dip directions. Following Okada *et al.* (2003), we carried out inversions with various maximum rupture velocities (from 2.6 to 5.0 km/s) to investigate which value was the most appropriate. For the evaluation function, we used the variance of the residuals (Mori and Hartzell, 1990):

$$\sigma^2 = \frac{|\mathbf{y} - \mathbf{A}\mathbf{x}|^2}{N_{\text{free}}}, \tag{7}$$

where **A** is the coefficient matrix, **x** is the model vector, and **y** is the data vector. N_{free} represents the degrees of freedom:

$$N_{\text{free}} = n\text{data} - n\text{sol} - 1, \tag{8}$$

where *n*data is the number of data and *n*sol is the number of parameters.

Figure 5 shows the change in the variance with respect to the maximum rupture velocity. The curves do not show clear minima, and the models with higher rupture velocity tend to show smaller variances. Such a result is sometimes seen in the multiple time-window analyses when the resolving power of the data is insufficient (for example, see table 3 in Hartzell and Heaton, 1983 for results obtained using only teleseismic data). This occurs because the number of effective unknown parameters at each timestep is proportional to the ruptured area, and the area becomes wider with increasing maximum rupture velocity; that is, the higher the

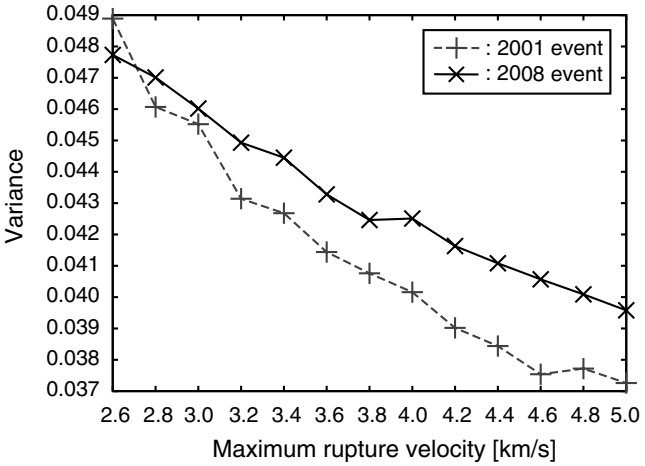

Figure 5. Relation between the maximum rupture velocity and variance of the residuals. Dashed gray curve is for the 2001 event; solid black curve is for the 2008 event.

maximum rupture velocity, the easier it becomes to explain the data. Thus, referring to Okada *et al.* (2003), we adopted 3.8 km/s for the maximum rupture velocity. If we use a higher velocity in the inversion, we obtain a slightly wider source area, but the characteristics of the slip distributions (shown in Fig. 6) are not altered. The moment rate function for each grid point was assumed to be expressed as a linear combination of four isosceles triangles with a base length of 0.06 s. We used a small event that occurred on 17 August 2001 (M 2.7) as the EGF. These parameters were used in the analyses for both the 2001 and 2008 events.

Figure 6 shows the slip distributions of the two events in map view, assuming a rigidity of 50 GPa. The slip distributions are superimposed so that the centroid of each distribution corresponds exactly to that estimated by Uchida *et al.* (2007, 2008), who located the centroids with an accuracy of ~20 m using the DD technique (Waldhauser and Ellsworth, 2000) and based on the cross spectra of the waveforms. Most of the two source areas overlap one another.

Analysis in the Frequency Range of 1.0–10.0 Hz

If we examine Figure 6 in more detail, we see that the slip distributions of the two events are slightly different. Moreover, the recurrence intervals and magnitudes of the repeating earthquakes off Kamaishi show minor fluctuations: the standard deviations of the recurrence interval and magnitude are 0.68 years and 0.1, respectively, indicating that the rupture process may also fluctuate.

Figure 7 shows examples of the waveforms of the 2001 and 2008 events, the differential waveform and the cross-correlation coefficient between the two events, and the lag time corresponding to the cross-correlation coefficient in the frequency ranges of 1.0–5.0 Hz (as used in the first analysis) and 1.0–10.0 Hz. We calculated the differential waveform by subtracting the waveform of the 2008 event from that of the 2001 event. Cross-correlation was calculated every 0.5 s using a moving time-window of 1.0 s.

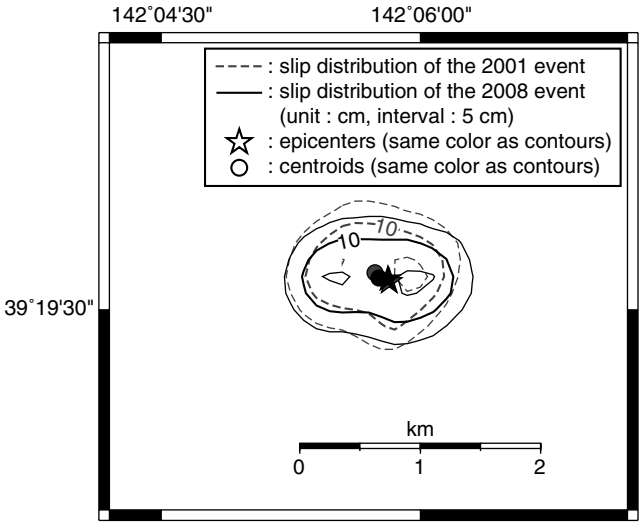

Figure 6. Slip distributions of the 2001 (dashed gray contours) and 2008 (solid black contours) events estimated from the seismograms in the frequency range of 1.0–5.0 Hz. The contour interval is 5 cm. Stars and circles indicate the epicenters and centroids, respectively, of the two events.

Even from the waveforms in the frequency range of 1.0–5.0 Hz, we can see slight differences between the 2001 and 2008 events in the high-frequency component. The differences are more clearly seen in the waveforms of 1.0–10.0 Hz. The cross-correlation coefficients show that the waveforms of the two events differ more in the frequency range of 1.0–10.0 Hz than in the range of 1.0–5.0 Hz. Therefore, as the next step, we analyzed band-pass-filtered seismograms in the frequency range of 1.0–10.0 Hz, to investigate differences in waveforms between the two events in the high-frequency range.

The method is the same as that described in the previous subsection, but the parameters are slightly changed because a higher resolution is required to investigate differences in waveforms between the two events in the 1.0–10.0 Hz frequency range. The parameters that are changed from the previous subsection are as follows. Waveform data were band-pass filtered with a frequency range of 1.0–10.0 Hz. For the fault plane, we assumed that the maximum size was 2.0×2.0 km^2. Grid points were placed on the fault plane with a spacing of 0.2 km in both the strike and dip directions. The moment rate function for each grid point was assumed to be expressed as a linear combination of six isosceles triangles with a base length of 0.04 s. Other parameters, such as the maximum rupture velocity (3.8 km/s), were kept the same as in the previous section.

Figure 8a,b,c shows snapshots of moment release distributions, total moment release distributions, and the moment rate function estimated for the 2001 event, respectively. Figure 9 contains the same plots for the 2008 event. Total moment release distributions for the two events (as shown by contours) define elliptical shapes elongated in the dip direction (east–west) (Figs. 8b and 9b). The shapes and the peak values of moment rate functions for the two events are similar to each other (Figs. 8c and 9c). Moreover, for both events the rupture duration times are estimated to be about 0.3 s.

For the 2001 event, the rupture propagated first from the hypocenter to the eastern (up-dip) part of the fault plane during the earlier stage (time-windows of 0.04–0.08 s); subsequently, the rupture accelerated to the western (down-dip) part, forming a symmetrical rupture pattern (time-windows of 0.08–0.12 s); finally, the rupture in the western area continued longer than that in the eastern area (time-windows of 0.12–0.16 to 0.20–0.24 s). For the 2008 event, on the other hand, the rupture propagated symmetrically from the hypocenter, in both the eastern and western directions, during the earlier stage (time-windows of 0.04–0.08 to 0.12–0.16 s), and the rupture in the western area continued longer than that in the eastern area (time-windows of 0.16–0.20 to 0.20–0.24 s).

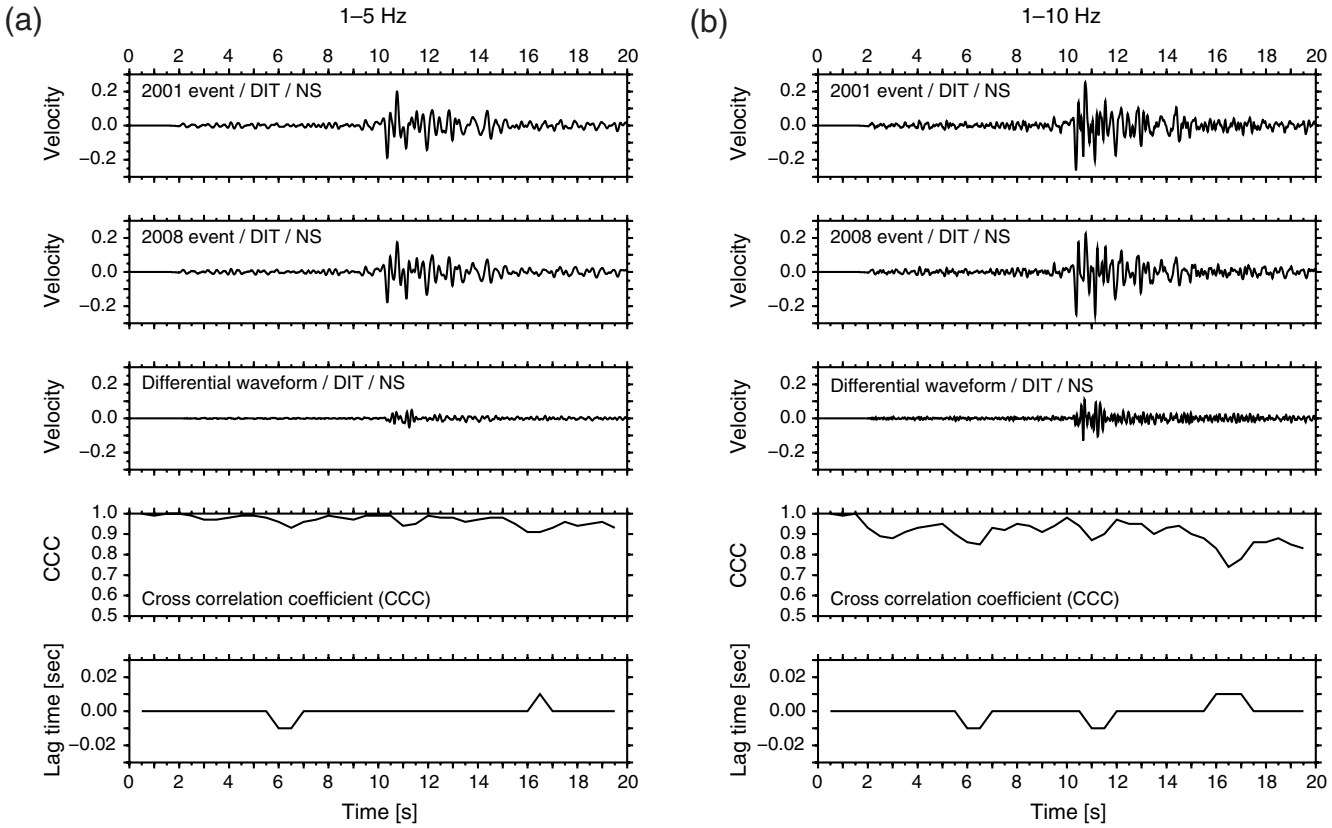

Figure 7. Examples of the waveforms for the 2001 and 2008 events, the differential waveform and the cross-correlation coefficient between the two events, and the lag time corresponding to the cross-correlation coefficient in the frequency range of (a) 1.0–5.0 Hz and (b) 1.0–10.0 Hz for the north–south component at station DIT. The differential waveforms were calculated by subtracting the waveform of the 2008 event from that of the 2001 event. The cross-correlations were calculated every 0.5 seconds using a moving time-window of 1.0 second. The cross-correlation coefficients and the lag times are plotted in the middle of the respective time-windows.

Figures 10 and 11 compare observed and synthetic waveforms for the 2001 and 2008 events, respectively. At some stations, the onsets in the synthetic waveforms appear to be faster than those in the observed ones, especially for *P* waves at stations FD2 and SN3. This is because the waveforms used as EGFs have rather poor signal-to-noise ratios for these stations. In both cases, however, the synthetic and observed waveforms are similar in the period after the *P*-wave arrivals.

Figure 12a shows the slip distributions of the two events in map view, assuming a rigidity of 50 GPa. In Figure 12a, the slip distributions of the two events are superimposed in the same way as in Figure 6. Most of the source areas overlap with each other, but their shapes are slightly different: the contours for the 2008 event show egg shapes elongated from east to west, while the contours for the 2001 event also form egg shapes, although these are wider in the eastern region.

The locations of the centroids of the two events are slightly different, but the hypocenters are almost the same. This result indicates that the slight difference in waveforms between the two events in the high-frequency range (see Fig. 7) was not caused by a difference in hypocenter locations (initial rupture points); instead, it was caused by slight differences in the rupture processes.

Discussion

Waveform inversions using an EGF method are thought to be affected by the selection of the small event used as the EGF (Okada *et al.*, 2003). To test the stability of the waveform inversion in this paper, we used a different small event as the EGF and inverted the data following the same procedure. We selected a small event with *M* 2.7 that occurred on 14 October 2001 (Table 1). Most of the two source areas (as obtained by using this small event as the EGF) also overlapped with each other, as in the case shown in Figure 12a (for details, see Ⓔ Fig. S3, available in the electronic supplement to this paper). This result clearly shows that the waveform inversion in this paper is stable. Thus, we conclude that the 2008 event was caused by rerupturing of the asperity (seismic patch) that caused the 2001 event, as predicted by Matsuzawa *et al.* (2002). Okada *et al.* (2003) showed that most of the source area for the 1995 event also overlapped with the source area for the 2001 event. The present result, and that of Okada *et al.* (2003), show that at least the last

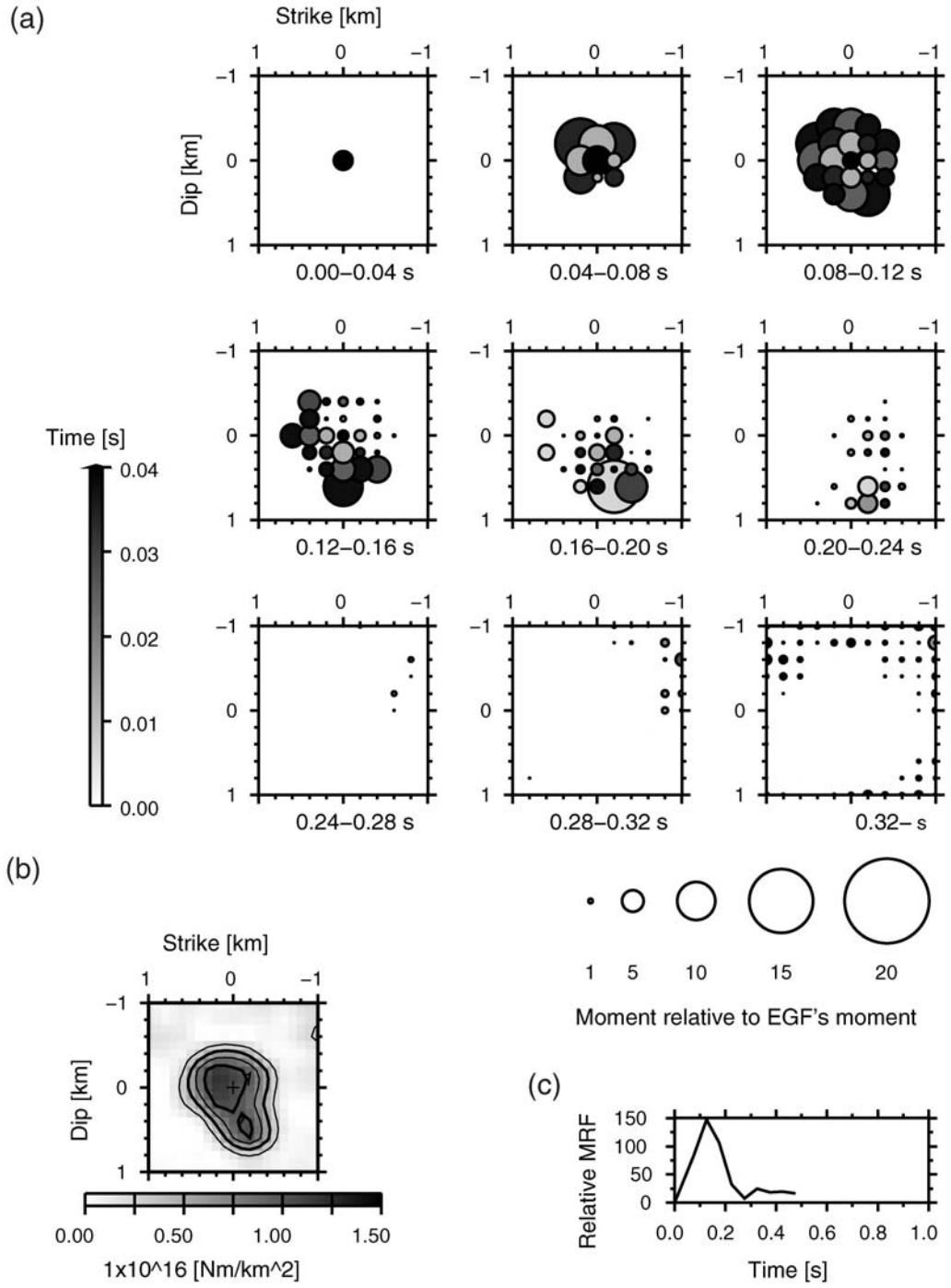

Figure 8. Results of inversion for the 2001 event for the frequency range of 1.0–10.0 Hz. (a) Snapshots of the moment release distribution. Time length for each window is 0.04 s. Diameter of each circle denotes the amount of moment release relative to the EGF's moment, and the tone of each circle indicates the time when the moment was released. Timescale for the snapshots is relative for every snapshot; that is, 0.00 s and 0.04 s correspond to the start time and end time of each time-window, respectively. (b) Total moment release distributions on the whole fault plane in units of 1×10^{16} N·m/km^2. (c) Moment rate function. Moment rates relative to the EGF are shown. In panels (a) and (b), the strike direction is 216° (south-southeast) and the dip direction is 31° downward from the horizontal. Along the dip axis, depth increases in the positive direction and decreases in the negative direction. Thus, these panels correspond to looking down the fault plane in the east-southeast direction from the hanging wall.

three events (1995, 2001, and 2008) in the off-Kamaishi repeating-earthquake sequence were caused by the repeated rupture of the same asperity patch.

Figure 12b shows the difference in the slip distribution between the 2001 and 2008 events. Generally, the 2001 event has greater slip than the 2008 event, but it has less slip in the

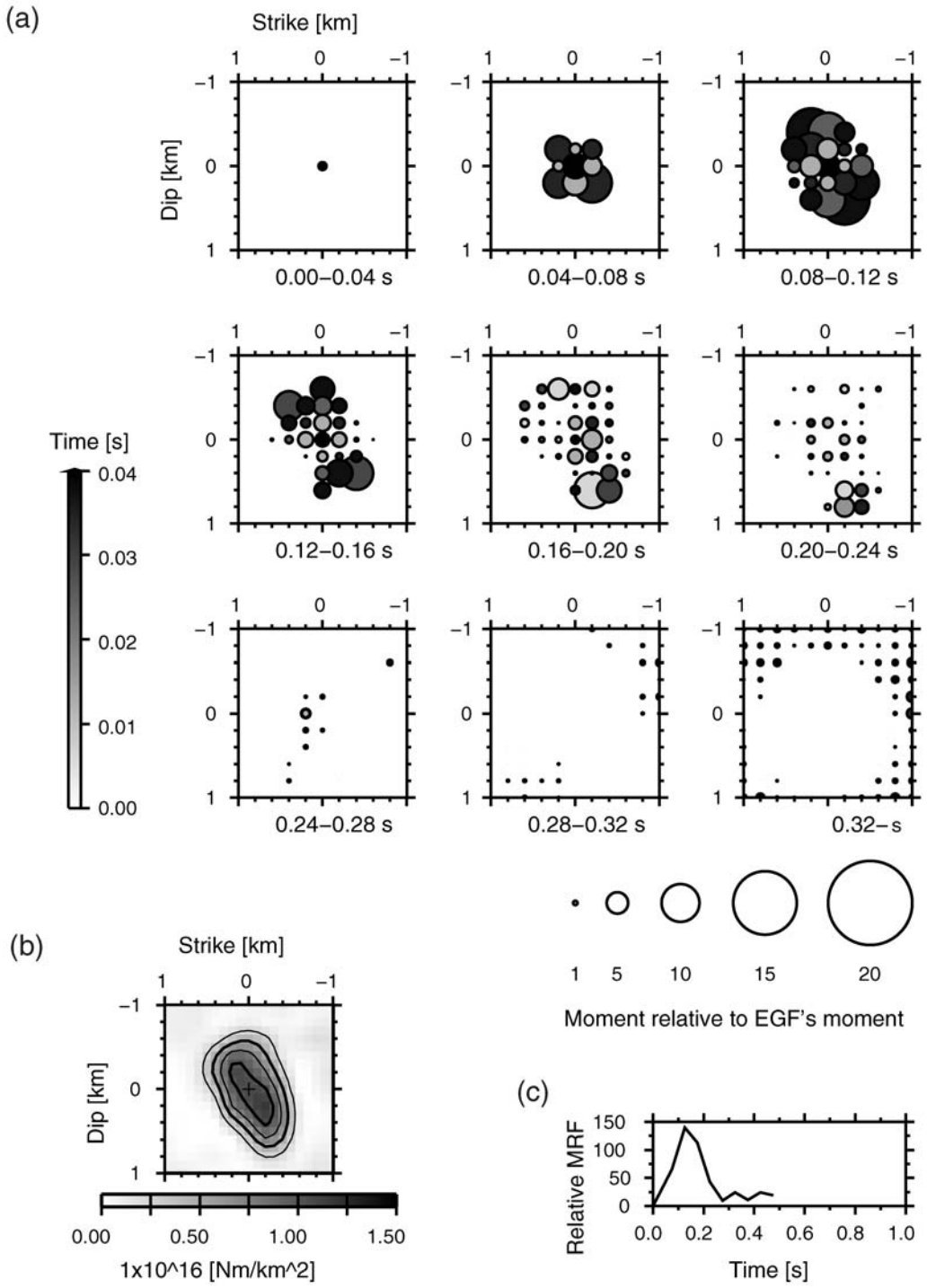

Figure 9. Same as for Figure 8, but for the 2008 event.

regions to the east and west of the epicenters. To test the stability of the pattern of the difference in slip amount between the 2001 and 2008 events, as shown in Figure 12b, we performed inversions using the jackknife method. In this method, inversions excluding one station were repeatedly performed, changing the excluded station each time. All the inversions show similar patterns of difference in the slip distribution between the 2001 and 2008 events (for details, see Ⓔ Fig. S4, available in the electronic supplement to this paper), indicating that the pattern shown in Figure 12b is reliable.

Uchida *et al.* (2007, 2008) estimated the centroids, radii of the rupture areas, and stress drops of the 2001 and 2008 events, and of smaller repeating earthquakes near the two events from spectral analyses (Fig. 12c,d). The slip amount of the 2001 event is greater than that of the 2008 event

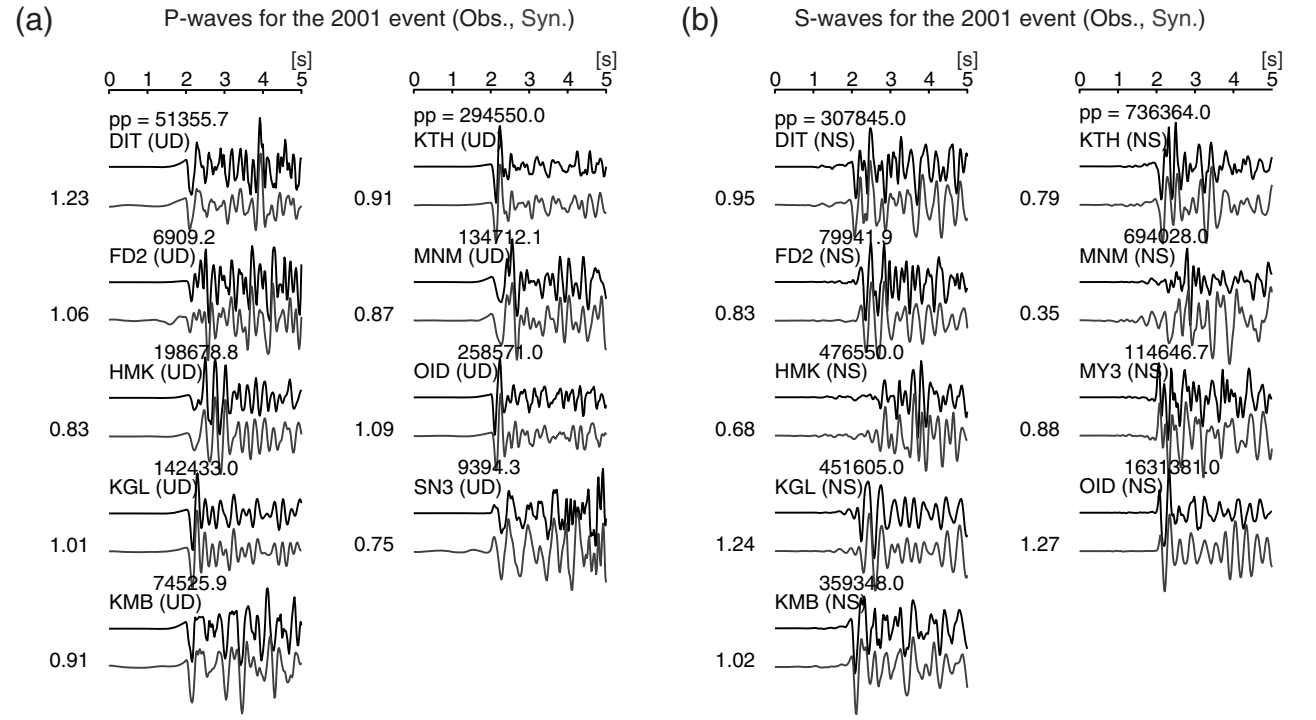

Figure 10. Examples of comparisons between observed and synthetic waveforms for the 2001 event for the frequency range of 1.0–10.0 Hz. Black and gray traces indicate observed and synthetic waveforms, respectively. Here, only seismograms of (a) the vertical-component for *P* waves and (b) the north–south component for *S* waves are shown (for the other components, see Ⓔ Fig. S1, available in the electronic supplement to this paper). The number above each pair of waveforms denotes the peak-to-peak amplitude of the observed waveform in 10^{-6} cm/s. The three-letter station code and component are also shown above each observed waveform. The number to the left of each pair of waveforms is the ratio of the maximum amplitude of the synthetic waveform to that of the observed waveform.

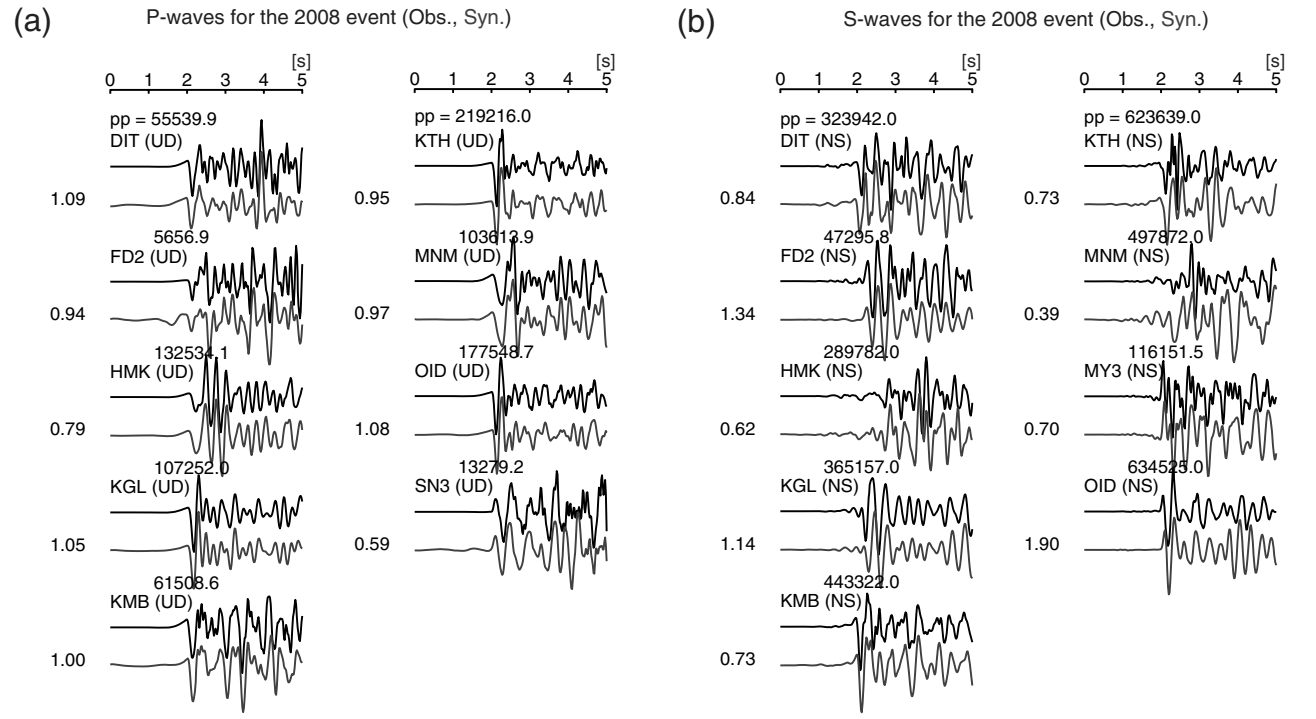

Figure 11. Same as for Figure 10, but for the 2008 event (for the other components, see Ⓔ Fig. S2, available in the electronic supplement to this paper).

because the recurrence interval before the 2001 event is longer (by about 0.5 years) than before the 2008 event (Fig. 1). This interpretation does not seem to apply to the 1995 event because the time interval before its occurrence is the shortest of the three events (i.e., among 1995, 2001, and 2008), while its Japan Meteorological Agency (JMA) magnitude of 5.0 is the largest. Based on careful estimates of the seismic moments, Okada *et al.* (2003) concluded that the seismic moment of the 2001 event is greater than that of the 1995 event. According to their results, the estimated seismic

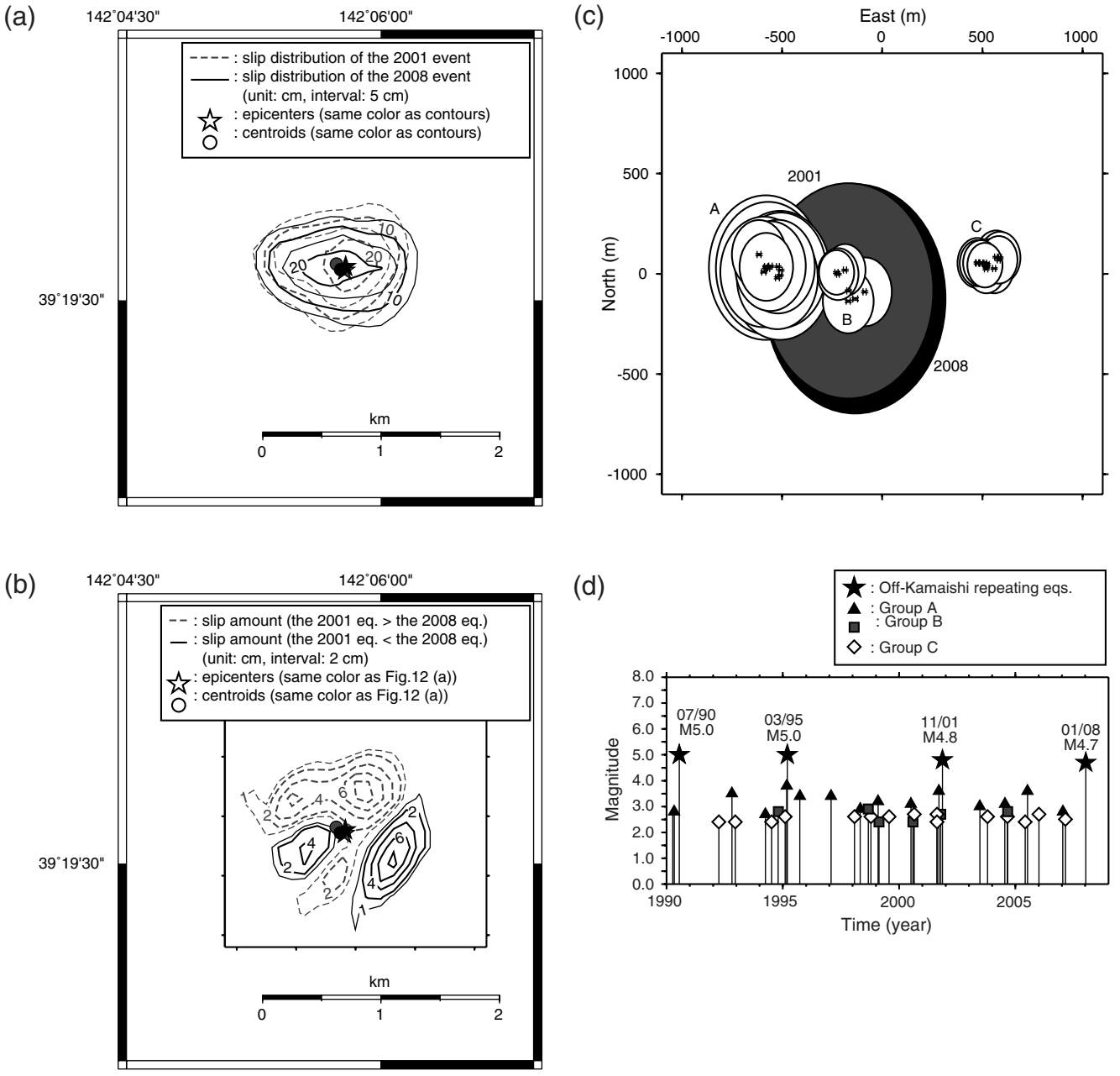

Figure 12. (a) Slip distributions of the 2001 (dashed gray contours) and 2008 (solid black contours) events estimated using the seismograms in the frequency range of 1.0–10.0 Hz. The contour interval is 5 cm. Stars and circles indicate the epicenters and centroids, respectively, of the two events. (b) Distribution of the difference in the slip amount between the 2001 and 2008 events, as calculated from (a). Dashed gray contours indicate that the slip amount of the 2001 event is greater than that of the 2008 event, and solid black contours indicate the opposite. The contour interval is 2 cm. Stars and circles indicate the epicenters and centroids, respectively, of the two events. Rectangular box shows the range shown in (c). (c) Centroids and radii of the rupture areas of the 2001 and 2008 events, and smaller repeating earthquakes near the two events (groups A, B, and C) for the period from April 1995 to January 2008, as estimated by Uchida *et al.* (2007, 2008), who assumed circular cracks on the subducting plate boundary for all events; the rupture areas become elliptical in this figure where the areas are projected onto the ground surface. (d) M-T diagram of the off-Kamaishi characteristic earthquake sequence (stars) and smaller repeating earthquakes (triangles for group A, squares for group B, and diamonds for group C) [Uchida *et al.* (2007, 2008)].

moments are 1.05×10^{16} N·m for the 1995 event and 1.11×10^{16} N·m for the 2001 event. Uchida *et al.* (2008) estimated the seismic moment of the 2008 event from the spectral ratios, assuming that the seismic moment of the 2001 event estimated by Okada *et al.* (2003) was correct. Their calculation yields a seismic moment for the 2008 event of 1.04×10^{16} N·m. The two sets of results indicate that the seismic moments for the 1995 and 2008 events are similar, slightly smaller than that for the 2001 event. We believe that this result reflects the long recurrence interval (the longest of the three events) before the 2001 event. However, we are considering fluctuations of less than 10% of the seismic moments, which corresponds to less than 0.1 of the moment magnitude and is comparable to the estimation error in the usual seismic moment estimation. Moreover, the moments are also affected by factors such as slip history, pore pressure, and the stressing rate (e.g., Ariyoshi *et al.*, 2007). Therefore, we do not consider why the 2001 event was the largest of the three events.

A comparison of the present results with the locations of smaller repeating earthquakes estimated by Uchida *et al.* (2007, 2008) shows both strong and weak correspondence of the areas with greater slip in the 2008 event to the locations of the nearby smaller repeating earthquakes. Strong correspondence is evident between the western area (with greater slip in the 2008 event) and the source areas of the smaller repeating earthquakes of groups A and B (Fig. 12b,c). On the other hand, the locations are slightly different between the eastern area and the smaller repeating earthquakes of group C. The difference is minor if we consider that the estimation error around the perimeter of the model space is usually larger than that close to the hypocenter. We checked the stability of the differences between the slip areas by changing the station selection, revealing that the overall pattern is insensitive to station selection, but the location of the peak of the eastern area of large slip shows a slight change (for details, see Ⓔ Fig. S4, available in the electronic supplement to this paper). Moreover, if we adopt a faster rupture velocity, the location of the peak moves toward the perimeter, as discussed earlier. All of these smaller repeating earthquakes (A, B, and C) were active just before the 2001 event but not active just before the 2008 event. Therefore, it is likely that the areas to the east and west of the mainshock epicenters show less slip in 2001 than in 2008 because the smaller repeating earthquakes occurred there just before the 2001 mainshock event (Fig. 12d).

Based on the asperity model, the source areas of the repeating earthquakes off Kamaishi and smaller repeating earthquakes (groups A, B, and C) are seismic patches, while their surrounding regions correspond to aseismically sliding areas (e.g., Boatwright and Cocco, 1996; Scholz, 1990). However, transition zones (i.e., weak seismic areas and compliant areas; Boatwright and Cocco, 1996) may exist between the seismic patches and surrounding aseismic regions. Such transition zones are usually active as slow-slip events or afterslip following nearby earthquakes, but may slip seismically if large seismic slip occurs at nearby large asperities (Boatwright and Cocco, 1996). If most of the eastern area of large slip in the 2008 event corresponds to the transition zone mentioned previously, the following scenario can be constructed. In the 2008 event, ruptures propagated toward the southeast and east (the location of group C), causing seismic slip in the transition zone. In the 2001 event, on the other hand, the transition zone did not slip seismically because it had slipped as afterslip following smaller events (group C) just before the 2001 event. This scenario also explains why the centroid of the 2008 event was located southeast of the 2001 event's centroid (see Fig. 5) and may explain why the eastern area of larger slip for the 2008 event does not correspond well to the location of group C events.

The cumulative slip amounts of the smaller repeating earthquakes (groups A and B) for the period before the 2001 event are estimated to be 2.8 and 1.7 cm, respectively (Uchida *et al.*, 2007, 2008), comparable to the peak value (~4 cm) of the difference in the slip distribution between the 2001 and 2008 events. This result indicates that we can estimate the slip distribution of a forthcoming large earthquake to some extent, just before its occurrence, based on the distribution of smaller events. Such an estimate may be useful for assessing the strong motions of large earthquakes.

Conclusions

To estimate the moment release distributions of the 2001 and 2008 repeating earthquakes off Kamaishi, we conducted multiple time-window waveform inversions with an empirical Green's function method, using three-component velocity-type seismograms obtained from Tohoku University's broadband-seismograph and microearthquake-observation networks.

In both events, ruptures propagated from the respective hypocenters to the east (up-dip) and to the west (down-dip) bilaterally, although during the 2001 event the ruptures in the west area continued for longer than in the east. As a result, the contours that show the distribution of total moment release are elliptical in shape, elongated east–west. The shapes and peak values of the moment rate functions for the two events are similar to each other, and most of the source areas of the two events overlap with each other.

From these results and those of Okada *et al.* (2003), we conclude that at least the last three events (1995, 2001, and 2008) were caused by the repeated rupture of the same asperity patch.

If we examine the events in more detail, however, we find that the 2008 event showed larger slip to the east and west of the epicenter, although the slip amount of the 2001 event was greater than that of the 2008 event. A comparison of these results with those of Uchida *et al.* (2007, 2008) indicates that the areas with greater slip in the 2008 event nearly correspond to the locations of the nearby smaller repeating earthquakes. Therefore, the difference in activity

between these smaller repeating earthquakes just before the 2001 and 2008 events probably influenced the observed fluctuations in the slip distribution of the repeating earthquakes off Kamaishi.

The present results indicate the occurrence of an asperity (seismic patch) on the plate boundary off Kamaishi, and earthquakes with $M \sim 5$ have regularly occurred on the asperity, as there are no nearby asperities of comparable size or larger. On the other hand, smaller repeating earthquakes are distributed in and around the asperity, and the activity of these smaller events just before the events off Kamaishi differ between the 2001 and 2008 events. Thus, the stress and strain distributions show slight differences in the asperity just before the occurrence of each mainshock. These differences probably cause the small fluctuations observed in the source process.

Data and Resources

Seismograms used in this paper were collected using Tohoku University's broadband-seismograph and microearthquake-observation networks and are not released to the public. Some figures were prepared using the Generic Mapping Tools version 4.4.0 (http://www.soest.hawaii.edu/gmt/; Wessel and Smith, 1998, last accessed April 2011) and Gnuplot version 4.0 (http://gnuplot.info/; Williams *et al.*, 2004, last accessed April 2011).

Acknowledgments

We thank two anonymous reviewers for their helpful and constructive comments and suggestions, which have greatly improved the paper.

References

Ariyoshi, K., T. Matsuzawa, R. Hino, and A. Hasegawa (2007). Triggered non-similar slip events on repeating earthquake asperities: Results from 3D numerical simulations based on a friction law, *Geophys. Res. Lett.* **34,** doi 10.1029/2006GL028323.

Boatwright, J., and M. Cocco (1996). Frictional constraints on crustal faulting, *J. Geophys. Res.* **101,** 895–909.

Ellsworth, W. L. (1995). Characteristic earthquakes and long-term earthquake forecasts: Implications of central California seismicity, in *Urban Disaster Mitigation: The Role of Science and Technology* F. Y. Cheng and M. S. Sheu (Editors), Elsevier, Oxford, 1–14.

Geller, R. J., and C. S. Mueller (1980). Four similar earthquakes in central California, *Geophys. Res. Lett.* **7,** 821–824.

Hartzell, S. (1978). Earthquake aftershocks as Green's functions, *Geophys. Res. Lett.* **5,** 1–4.

Hartzell, S., and T. Heaton (1983). Inversion of strong ground motion and teleseismic waveform data for the fault rupture history of the 1979 Imperial Valley, California, earthquake, *Bull. Seismol. Soc. Am.* **73,** 1553–1583.

Hasegawa, A., N. Umino, and A. Takagi (1978). Double-planed structure of the deep seismic zone in the northeastern Japan arc, *Tectonophysics* **47,** 43–58.

Hori, T., and S. Miyazaki (2010). Hierarchical asperity model for multiscale characteristic earthquakes: A numerical study for the off-Kamaishi earthquake sequence in the NE Japan subduction zone, *Geophys. Res. Lett.* **37,** doi 10.1029/2010GL042669.

Igarashi, T., T. Matsuzawa, and A. Hasegawa (2003). Repeating earthquakes and interplate aseismic slip in the northeastern Japan subduction zone, *J. Geophys. Res.* **108,** doi 10.1029/2002JB001920.

Kanamori, H. (1981). The nature of seismicity patterns before large earthquakes, in *Earth Prediction: An international review*, D. W. Simpson and P. G. Richards (Editors), Maurice Ewing Ser. **4**, AGU, Washington, D.C., 1–19.

Konca, A. O., J-P. Avouac, A. Sladen, A. J. Meltzner, K. Sieh, P. Fang, Z. Li, J. Galetzka, J. Genrich, M. Chlieh, D. H. Natawidijaja, Y. Bock, E. J. Fielding, C. Ji, and D. V. Helmberger (2008). Partial rupture of a locked patch of the Sumatra megathrust during the 2007 earthquake sequence, *Nature* **456,** doi 10.1038/nature07572.

Lay, T., and H. Kanamori (1980). Earthquake doublets in the Solomon Islands, *Phys. Earth Planet. Inter.* **21,** 283–304.

Lay, T., and H. Kanamori (1981). An asperity model of large earthquake sequences, in *Earth Prediction: An International Review* D. W. Simpson and P. G. Richards (Editors), Maurice Ewing Ser. **4,** AGU, Washington, D.C., 579–592.

Lay, T., H. Kanamori, and L. Ruff (1982). The asperity model and the nature of large subduction zone earthquakes, *Earthquake Pred. Res.* **1,** 3–71.

Matsuzawa, T., T. Igarashi, and A. Hasegawa (1999). Characteristic small-earthquake sequence off Sanriku, Japan, *Eos Trans. AGU* **80,** no. 46, F724.

Matsuzawa, T., T. Igarashi, and A. Hasegawa (2002). Characteristic small-earthquake sequence off Sanriku, northeastern Honshu, Japan, *Geophys. Res. Lett.* **29,** doi 10.1029/2001GL014632.

Mori, J., and S. Hartzell (1990). Source inversion of the 1998 Upland, California, earthquake: Determination of a fault plane for a small event, *Bull. Seismol. Soc. Am.* **80,** 507–518.

Nadeau, R. M., and T. V. McEvilly (1997). Seismological studies at Parkfield V: Characteristic microearthquakes sequence as fault-zone drilling targets, *Bull. Seismol. Soc. Am.* **87,** 1463–1472.

Nadeau, R. M., W. Foxall, and T. V. McEvilly (1995). Clustering and periodic recurrence of microearthquakes on the San Andreas fault at Parkfield, California, *Science* **267,** 503–507, doi 10.1126/science.267.5197.503.

Nagai, R., M. Kikuchi, and Y. Yamanaka (2001). Comparative study on the source process of recurrent large earthquakes in Sanriku-oki region: The 1968 Tokachi-oki earthquake and the 1994 Sanriku-oki earthquake, *J. Seismol. Soc. Jpn.* **52,** 267–289 (in Japanese with English abstract).

Okada, T., T. Matsuzawa, and A. Hasegawa (2003). Comparison of source areas of $M4.8 + / - 0.1$ repeating earthquakes off Kamaishi, NE Japan: Are asperities persistent features? *Earth Planet. Sci. Lett.* **213,** 361–374.

Park, S. C., and J. Mori (2007). Are asperity patterns persistent? Implication from large earthquakes in Papua New Guinea, *J. Geophys. Res.* **112,** doi 10.1029/2006JB004481.

Scholz, C. H. (1990). *The Mechanics of Earthquakes and Faulting*, Cambridge Univ. Press, New York.

Uchida, N., T. Matsuzawa, W. L. Ellsworth, K. Imanishi, T. Okada, and A. Hasegawa (2007). Source parameters of a *M* 4.8 and its accompanying repeating earthquakes off Kamaishi, NE Japan: Implications for the hierarchical structure of asperities and earthquake cycle, *Geophys. Res. Lett.* **34,** L20313, doi 10.1029/2007GL031263.

Uchida, N., T. Matsuzawa, T. Okada, K. Shimamura, A. Hasegawa, K. Imanishi, and W. L. Ellsworth (2008). The 2008 off-Kamaishi repeating earthquake and micro earthquake activity around the event, *JPGU 2008 Meeting*, S142-007 (in Japanese with English abstract).

Waldhauser, F., and W. L. Ellsworth (2000). A double-difference earthquake location algorithm: Method and application to the northern Hayward fault, California, *Bull. Seismol. Soc. Am.* **90,** 1353–1368, doi 10.1785/0120000006.

Wessel, P., and W. H. F. Smith (1998). New, improved version of Generic Mapping Tools released, *Eos Trans. AGU* **79,** 579.

Williams, T., C. Kelley, H.-B. Bröker, J. Campbell, R. Cunningham, D. Denholm, G. Elber, R. Fearick, C. Grammes, L. Hart, L. Hecking, T. Koenig, D. Kotz, E. Kubaitis, R. Lang, A. Lehmann, A. Mai, E. A. Merritt, P. Mikulik, C. Steger, T. Tkacik, J. V. der Woude, A. Woo, J. R. V. Zandt, and J. Zellner (2004). *Gnuplot—An Interactive Plotting Program*, ver. **4.0,** http://gnuplot.info/.

Wu, C., K. Koketsu, and H. Miyake (2008). Source processes of the 1978 and 2005 Miyagi-oki, Japan, earthquakes: Repeated rupture of asperities over successive large earthquakes, *J. Geophys. Res.* **113,** doi 10.1029/2007JB005189.

Yagi, Y. (2004). Source rupture process of the 2003 Tokachi-oki earthquake determined by joint inversion of teleseismic body wave and strong ground motion data, *Earth Planets Space* **56,** 31–316.

Yaginuma, T., T. Okada, A. Hasegawa, K. Kato, M. Takemura, and Y. Yagi (2007). Coseismic slip distribution of the 2005 Miyagi-Oki (*M* 7.2) earthquake estimated by inversion of strong-motion and teleseismic waveforms—Its relation with the 1978 Miyagi-Oki earthquake (*M* 7.4), *J. Seismol. Soc. Jpn.* **60,** 43–53 (in Japanese with English abstract).

Yamanaka, Y., and M. Kikuchi (2003). Source process of the recurrent Tokachi-oki earthquake on September 26, 2003, inferred from teleseismic body waves, *Earth Planets Space* **55,** e21–e24.

Yamanaka, Y., and M. Kikuchi (2004). Asperity map along the subduction zone in northeastern Japan inferred form regional seismic data, *J. Geophys. Res.* **109,** doi 10.1029/2003JB002683.

Research Center for Prediction of Earthquakes and Volcanic Eruptions
Graduate School of Science
Tohoku University
6-6 Aza-Aoba, Aramaki, Aoba-ku
Sendai 980-8578, Japan
shimamura@aob.gp.tohoku.ac.jp
(K.S., T.M., T.O., N.U., A.H.)

Tono Seismological Observatory
Research Center for Prediction of Earthquakes and Volcanic Eruptions
Graduate School of Science
Tohoku University
4-120-74 Komagi, Matsuzaki-cho
Tono 028-0545, Japan
(T.K.)

Manuscript received 25 October 2010